Effects of material composition on the superlens frequency of photonic crystals

XiaoHong Sun,[1,2] XiaoMing Tao,[1,*] and KaiCheong Kwan[1]

[1]*Institute of Textiles and Clothing, The Hong Kong Polytechnic University, Hung Hom, Kowloon, Hong Kong*
[2]*E-mail: tcsunxh@polyu.edu.hk*
**Corresponding author:tctaoxm@inet.polyu.edu.hk*

Received November 16, 2007; accepted January 21, 2008;
posted February 6, 2008 (Doc. ID 89812); published March 26, 2008

We use the plane-wave (PW) method to calculate the superlens frequency of photonic crystals with various material compositions. At this frequency, photonic crystal behaves like a medium with isotropic negative index equal to −1. The relationship between the frequency and material compositions is derived from the calculated data. For the TE and TM modes, the relationship has the same format. From the relationship, a case has been chosen and, under these conditions, the wave-propagating field through the photonic crystal has been calculated by the finite-difference time-domain method. A good agreement is obtained between the results from the PW method and the finite-difference time-domain calculation. This is very useful for fabricating photonic crystal superlens material at an appropriate frequency. © 2008 Optical Society of America

OCIS codes: 160.5298, 160.3918, 220.4610, 220.4830, 230.3990, 230.5298.

1. INTRODUCTION

Recently, materials exhibiting negative refraction have attracted considerable attention as stimulated by the seminal work of Veselago [1–3]. These structures are periodic and can be realized with so-called metamaterials [4–6] or photonic crystals (PhCs). Depending on the product sign of $\boldsymbol{v}_{ph} \cdot \boldsymbol{v}_{gr}$ in PhCs, we distinguish the right-handed (positive sign) and left-handed negative refraction (negative sign) [7] ($\boldsymbol{v}_{ph}$ and $\boldsymbol{v}_{gr}$ are the phase and group velocities in PhC). Right-handed all-angle negative refraction (AANR) was proved by Luo *et al.* [8] in the vicinity of the M point of the first band of 2D square lattice PhCs with air holes in GaAs dielectric background, in which equifrequency contours (EFCs) are convex with inward gradients toward the M point. AANR material at $n=-1$ is an excellent material for superlens applications that can potentially overcome the diffraction limit inherent in conventional lenses [9]. The left-handed negative refraction is also possible in PhCs in higher bands around the Γ point [10,11]. There, $\boldsymbol{v}_{ph}$ and $\boldsymbol{v}_{gr}$ can be antiparallel like those in Veselago's metamaterials. All-angle left-handed negative refraction (AALNR) in 2D Kagome and honeycomb lattices made of dielectric rods in air was discussed by Gajic *et al.* [12]. In these PhC structures, AANR happens at $n_{\mathrm{eff}}=-1$, where n_{eff} is the effective index of PhC. In all these references, negative refraction is considered for a given dielectric constant and filling factor. It is highly desirable to know the relationship between superlens frequency (AANR frequency at $n=-1$) and dielectric constant and filling factor so that AANR superlens material can be designed and fabricated at an appropriate frequency.

In this paper, the plane wave (PW) method is used to calculate 2D triangular lattice PhC band structure and EFCs. The superlens frequency is determined for different dielectric constants and filling factors. The relationship between these parameters is derived from these data. For the TE and TM modes (the electric field and magnetic field are parallel to the rods for the TM and TE modes, respectively), the relationship has the same format. For example, with a given filling factor and dielectric constant, the wave propagating field through the PhC has been calculated by the finite-difference time-domain (FDTD) method. A good agreement is obtained between the derived results by the PW method and FDTD calculation.

2. CALCULATION OF 2D PHOTONIC CRYSTAL NEGATIVE REFRACTION

The PW method [13] is used to calculate the band diagram and EFCs for a slab or film that consists of an array of infinitely long, parallel, air rods ($\varepsilon_a=1$), each with a circular cross section of radius r, embedded in a background dielectric material ($n=2.65$ or $\varepsilon_b=7$). The intersections of these rods with the perpendicular plane formed a triangular lattice. In calculation, Bloch waves are expanded by approximately 441 PWs. FDTD [14–16] calculations were used to analyze the electromagnetic wave propagation through PhCs. Calculations were performed for TM bands of PhCs where left-handed negative refraction took place.

The first five bands, as shown in Fig. 1, are calculated with a filling factor of $f=2\pi r^2/\sqrt{3}a^2=0.8358$ [17] (or $r=0.48a$; a is the lattice constant). To avoid high-order diffraction [8], only band 2 is considered, whose EFCs are shown in Fig. 2. The EFC structure reveals that when the frequencies are close to the central point (the band edges), the shapes of EFCs are almost circular. That is to say, the

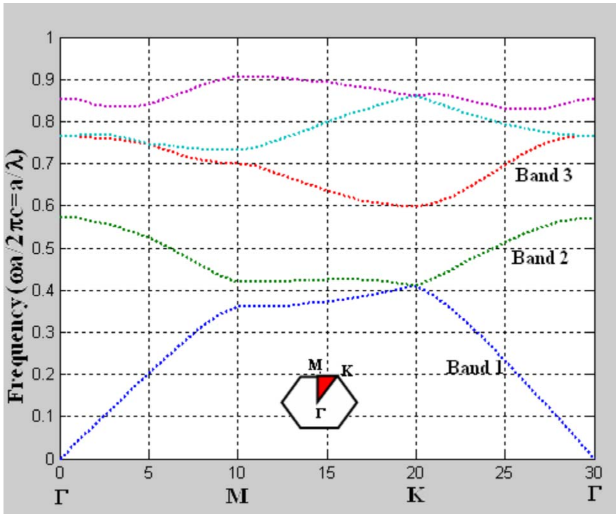

Fig. 1. (Color online) TM band structure of a 2D PhC with a filling factor $f=0.8358$, $\varepsilon_a=1$, and $\varepsilon_b=7$ in the first Brillouin zone.

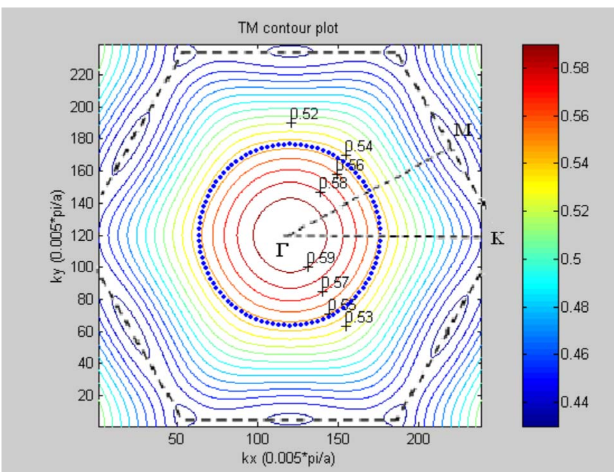

Fig. 2. (Color online) Equifrequency contours of band 2 with a filling factor $f=0.8358$, $\varepsilon_a=1$, and $\varepsilon_b=7$ in the first Brillouin zone; circle with the blue dashed line shows $\bar{\omega}=0.564$ in air.

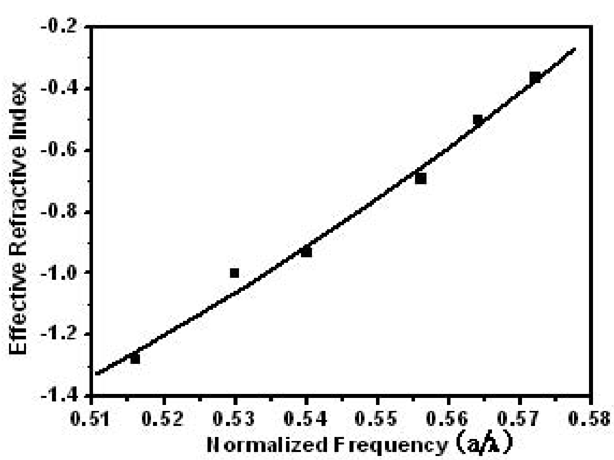

Fig. 3. Effective refractive index versus normalized frequency in band 2 with a filling factor $f=0.8358$, $\varepsilon_a=1$ and $\varepsilon_b=7$. Squares indicate the calculated results.

relationship between the frequency ω and wave-vector k is linear, $\omega=|v_p k|=ck/|n_p|=c(k_x^2+k_y^2)^{1/2}/|n_p|=cR(\omega)/|n_p|$ [10], where $R(\omega)$ is the radius of EFCs. Then we can obtain the effective phase index $n_p=R(\omega)/R_0(\omega)$, where $R(\omega)$ and $R_0(\omega)$ are the radii of EFC of frequency ω in the PhC and air, respectively. The calculated effective index (squares) of band 2 is shown in Fig. 3, which illustrates a normal dispersion curve. From the curve, at $\bar{\omega}=0.534$, the effective refractive index is $n=-1$. In other words, $\bar{\omega}=0.534$ is the central frequency of AALNR.

In the same way, the effective refractive indices (squares) of band 2 are calculated for various filling factors of 0.58 ($r=0.4a$), 0.444 ($r=0.35a$), 0.326 ($r=0.3a$), and 0.145 ($r=0.2a$), as shown in Figs. 4(a)–4(d), respectively, where the derived central frequencies of AALNR are 0.428, 0.405, 0.391, and 0.379, respectively. From these data (squares), the relationship between AALNR frequency and the filling factor can be obtained for the ratio of dielectric constant (RDC) $\varepsilon_b/\varepsilon_a=7$, as shown in Fig. 5. The curve is represented by a polynomial regression equation

$$y=0.3814-0.08111x+0.56191x^2-0.9229x^3+0.75157x^4, \tag{1}$$

where y and x stand for the frequency a/λ and filling factor, respectively. The AALNR frequency is increased monotonically with the filling factor. The correlation coefficient is $R=0.99999$.

Similarly, AALNR frequencies for different RDCs and filling factors are calculated. The multiregression result of the calculated data (dots) is shown in Fig. 6, depicting that these data are well-fitted in one surface. The regression function is

$$z(x,y)=\sum_{i=0}^{3}\sum_{j=0}^{3}a_{ij}x^i y^j. \tag{2}$$

The values of a_{ij} are given in Table 1. x and y stand for RDC and filling factor, respectively. This is a quadric function. The sum of deviations squared of the least-square fitting is $\delta=\sum_{k=l}^{n}\sum_{l=l}^{n}w(x_k,y_l)[z(x_k,y_l)-f(x_k,y_l)]^2=5.3964\times10^{-5}$, where $w(x_k,y_l)$ is a weight function and set as 1, $z(x_k,y_l)$ and $f(x_k,y_l)$ are the value of the fitted function and data point at coordinate (x_k,y_l), respectively, and $n=6$ is the number of coordinate x or y. The surface projection curves in the plane of the RDC and the filling factor are also indicated, i.e., for a certain AANR frequency the values of the RDC and the filling factor are obtained from these curves. Furthermore, the larger the AALNR frequency is, the smaller the range of values of the RDC and the filling factor.

As an example, a PhC with a filling factor of $f=0.6$, the AALNR frequency $\bar{\omega}=0.434$ from Eq. (1) is used in the calculation. The effective index of this point is $n=-1$. The wave pattern of the TM electromagnetic wave propagating through the PhC at an incident angle 20° to the ΓM surface is calculated by using the FDTD method and is presented in Fig. 7. The Gaussian line source with a pulse width of −0.1 is used in the calculation. Figure 7(a) shows the PhC structure and 7(b) illustrates that the incident

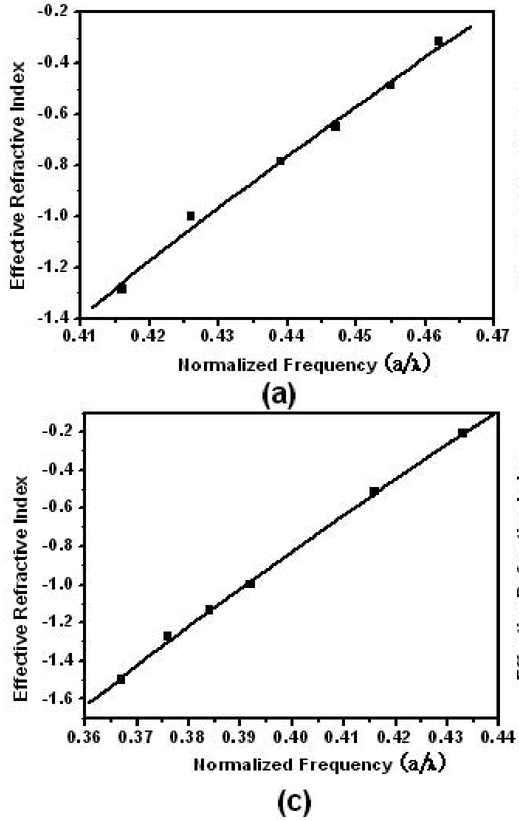

Fig. 4. Effective refractive index versus normalized frequency at filling factor (a) 0.58 ($R=0.4a$), (b) 0.444 ($R=0.35a$), (c) 0.326 ($R=0.3a$), and (d) 0.145 ($R=0.2a$). Squares indicate the calculated results.

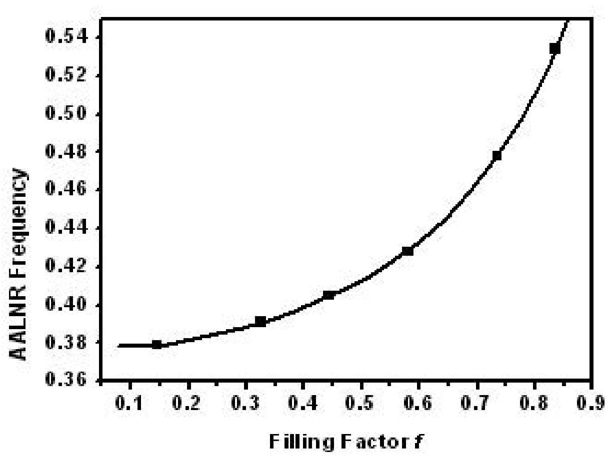

Fig. 5. AANR frequency versus filling factor with $\varepsilon_b/\varepsilon_a=7$. Squares indicate the calculated results.

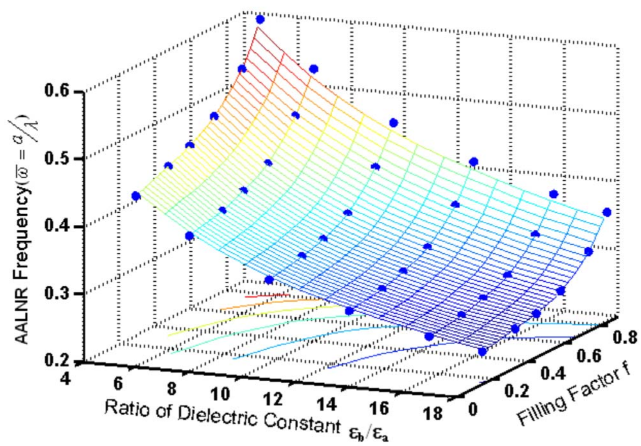

Fig. 6. (Color online) AALNR frequency of TM mode as a function of RDC and filling factor. The dots and meshed surface represent the calculated and fitted result, respectively.

and output light are parallel. This indicates that the effective index should be $n=-1$.

The above analysis illustrates the effectiveness of the PW and FDTD methods in derivation of the relationship between AALNR frequency, the RDC, and filling factor for 2D PhCs of triangular lattice. These methods can be applied to other 2D PhC structures, i.e., square lattice, honeycomb lattice, etc. In addition, the present FDTD method can be extended to calculate EFCs to obtain the relationship for metal or hybrid PhC structures.

Table 1. Coefficients in Regression Equation (2) for AALNR Frequencies of TM Mode

a_{ij}	0	1	2	3
0	0.53431	0.81905	−1.5628	1.2246
1	−0.033519	−0.15326	0.27437	−0.15887
2	0.0013203	0.011474	−0.021343	0.012175
3	−2.2663e−005	−0.00026843	0.00051281	−0.00029585

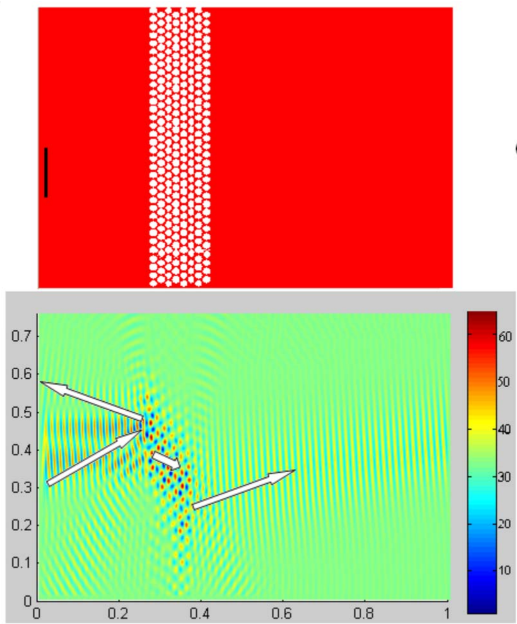

Fig. 7. (Color online) (a) PhC structure and the (b) wave pattern of $\bar{\omega}=0.434$ TM electromagnetic wave propagating through the PhC as an incident angle 20° to the ΓM surface.

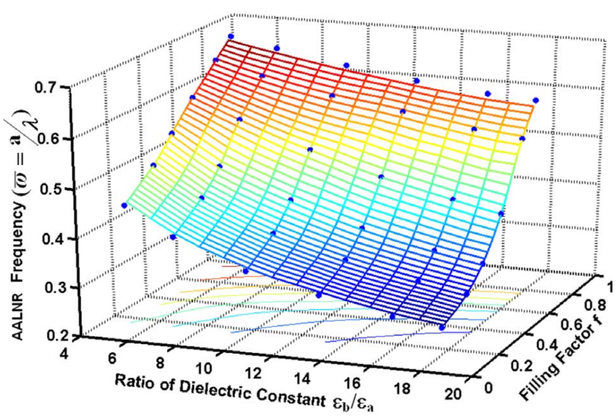

Fig. 8. (Color online) AALNR frequency of TE mode as a function of RDC and filling factor. The dots and meshed surface represent the calculated and fitted result, respectively.

Table 2. Coefficients in Regression Equation (2) for AALNR Frequencies of TE Mode

a_{ij}	0	1	2	3
0	0.53297	1.1533	−2.1345	1.2391
1	−0.028088	−0.2941	0.75699	−0.45501
2	0.0014605	0.016592	−0.045958	0.028933
3	−3.459e−005	−0.00029698	0.00085176	−0.00052743

In the same way, the relationship between the AALNR frequency and the RDC and the filling factor for the TE mode is also derived and has the same format as Eq. (2) for the TM mode. The multiregression result of the calculated data (blue dots) is shown in Fig. 8, depicting that these data are well fitted in one surface. The regression coefficients are shown in Table 2. The sum of deviations squared of the least-square fitting is $\delta=\sum_{k=1}^{n}\sum_{l=1}^{n}w(x_k,y_l)\times[z(x_k,y_l)-f(x_k,y_l)]^2=6.5858\times10^{-4}$. The AANR frequency is also increased with the increase of the filling factor and the decrease of the RDC.

From the calculated results, an appropriate superlens structure can be designed. For example, we can use the structure $r=0.48a$, $a=338$ nm with $\varepsilon_a=1$ and $\varepsilon_b=7$ to realize superlens at the visible wavelength 632 nm.

3. CONCLUSION

In this paper, the plane-wave (PW) method has been used to calculate PhC band structure and equifrequency contour and obtain the AALNR frequency or wavelength for PhC structures with different dielectric constant and filling factor. A regression relationship between AALNR frequency, filling factor, and dielectric constant has been derived from these data. For TE and TM modes, the relationship has the same format. For example, with a given filling factor and dielectric constant, the wave propagating field through the PhC film has been calculated by the finite-difference time-domain (FDTD) method. A good agreement is obtained between the derived results by the PW method and FDTD calculation. This relationship is very useful for designing and fabricating AALNR material at an appropriate frequency or wavelength.

ACKNOWLEDGMENTS

X.-H. Sun acknowledges a postdoctoral fellowship from the Hong Kong Polytechnic University (G-YX67). K.-C. Kwan acknowledges a postgraduate scholarship from the same source.

REFERENCES

1. V. G. Veselago, “Electrodynamics of substances with simultaneously negative electrical and magnetic permeabilities,” Usp. Fiz. Nauk **92**, 517–526 (1967).
2. V. G. Veselago, “The electrodynamics of substances with simultaneously negative values of ε and μ,” Sov. Phys. Usp. **10**, 509–514 (1968).
3. V. G. Veselago, “Electrodynamics of materials with negative index of refraction,” Usp. Fiz. Nauk **173**, 790–794 (2003).
4. J. B. Pendry and D. R. Smith, “Reversing light with negative refraction,” Phys. Today **57**, 37–43 (2004).
5. J. B. Pendry, A. J. Holden, D. J. Robbins, and W. J. Stewart, “Magnetism from conductors and enhanced nonlinear phenomena,” IEEE Trans. Microwave Theory Tech. **47**, 2075–2084 (1999).
6. R. A. Shelby, D. R. Smith, and S. Schultz, “Experimental verification of a negative index of refraction,” Science **292**, 77–79 (2001).
7. R. Gajic, R. Meisels, F. Kuchar, and K. Hingerl, “Refraction and rightness in photonic crystals,” Opt. Express **13**, 8596–8604 (2005).
8. C. Luo, S. G. Johnson, J. D. Joannopoulos, and J. B. Pendry, “All-angle negative refractive without negative effective index,” Phys. Rev. B **65**, 201104(R) (2002).
9. J. B. Pendry, “Negative refraction makes a perfect lens,” Phys. Rev. Lett. **85**, 3966–3969 (2000).
10. M. Notomi, “Theory of light propagation in strongly modulated photonic crystals: refractionlike behavior in the vicinity of the photonic band gap,” Phys. Rev. B **62**, 10696 (2000).

11. S. Foteinopoulou and C. M. Soukoulis, “Negative refraction and left-handed behavior in two-dimensional photonic crystals,” Phys. Rev. B **67**, 235107 (2003).
12. R. Gajic, R. Meisels, F. Kuchar, and K. Hingerl, “All-angle left-handed negative refraction in Kagome and honeycomb lattice photonic crystals,” Phys. Rev. B **73**, 165310 (2006).
13. S. P. Guo and S. Albin, “Simple plane wave implementation for photonic crystal calculations,” Opt. Express **11**, 167–175 (2003).
14. M. Qiu, “Effective index method in heterostructure slab waveguide based two-dimensional photonic crystals,” Appl. Phys. Lett. **81**, 1163–1165 (2002).
15. M. Qiu, B. Jaskorzynska, M. Swillo, and H. Benisty, “Time-domain 2D modeling of slab-waveguide based photonic-crystal devices in the presence of out-of-plane radiation losses,” Microwave Opt. Technol. Lett. **34**, 387–393 (2002).
16. M. Qiu, F2P: Finite-difference time-domain 2D simulator for Photonic devices, http://www.imit.kth.se/info/FOFU/PC/F2P/.
17. M. Plihal and A. A. Maradudin, “Photonic band structure of two-dimensional systems: the triangular lattice,” Phys. Rev. B **44**, 8565–8571 (1991).